

Stator Winding Fault Detection of Permanent Magnet Synchronous Motors Based on the Short-Time Fourier Transform

Research paper

Przemysław Pietrzak^{1b}, Marcin Wolkiewicz*^{1b}

Wrocław University of Science and Technology, 50-370 Wrocław, Poland

Received: May 05, 2022; Accepted: June 02, 2022

Abstract: In modern drive systems, the high-efficient permanent magnet synchronous motors (PMSMs) have become one of the most substantial components. Nevertheless, such machines are exposed to various types of faults. Hence, on-line condition monitoring and fault diagnosis of PMSMs have become necessary. One of the most common PMSM faults is the stator winding fault. Due to the destructive character of this failure, it is necessary to use fault diagnostic methods that allow fault detection at its early stage. The article presents the results of experimental studies obtained from fast Fourier transform (FFT) and short-time Fourier transform (STFT) analyses of the stator phase current, stator phase current envelope and stator phase current space vector module. The superiority of the proposed method over the classical approach based on the stator current analysis using FFT is highlighted. The proposed solution is experimentally verified under various motor operating conditions. The application of STFT analysis discussed so far in the literature has been limited to the fault diagnosis of induction motors and the narrow range of the analysed motor operating conditions. Moreover, there are no works in the field of motor diagnostics dealing with STFT analysis for stator windings based on the stator current envelope and the stator current space vector module.

Keywords: faults diagnosis • condition monitoring • inter-turn short circuit • permanent magnet synchronous motor • short-time Fourier transform

1. Introduction

The significant advantages of permanent magnet synchronous motors (PMSMs), such as very high efficiency, high power density, wide speed range and reliability, have led to their frequent use in many drive systems nowadays (Pietrzak and Wolkiewicz, 2021c). PMSMs have been widely utilized in various fields, such as aerospace, automotive, home appliances, HVAC and robotics (Zhou et al., 2021).

Despite the high reliability of PMSMs, various types of faults of these machines may occur. Motor fault can result in stopping various operational activities of a company leading to the significant loss and so its diagnosis is becoming an increasingly important issue (Tarchała et al., 2020). The PMSM faults can be divided into mechanical, electrical and magnetic damages. Stator winding faults account for 21%–40% of all electric motor failures, depending on the type and size of the machine (Riera-Guasp et al., 2015). Failures of stator winding begin mainly as imperceptible short circuit of single turns – inter-turn short circuit (ITSC), and in consequence spread over the whole winding (Wolkiewicz et al., 2016). This type of damage is very destructive. ITSCs can lead to a phase-to-phase and phase-to-ground short circuit. In addition, the ITSC in the PMSM stator winding is a source of local temperature rise resulting from short-circuit currents with very high value that may damage the permanent magnet (Skowron et al., 2022). The four types of PMSM stator winding short circuits are shown in Figure 1.

Due to the destructive nature of the PMSM stator winding fault, it must be detected at an early stage to prevent the fault spreading. Early detection can significantly reduce machine repair costs. Therefore, the implementation of an appropriate diagnostic system, based on effective algorithms, is essential to prevent complete failure of

* Email: marcin.wolkiewicz@pwr.edu.pl

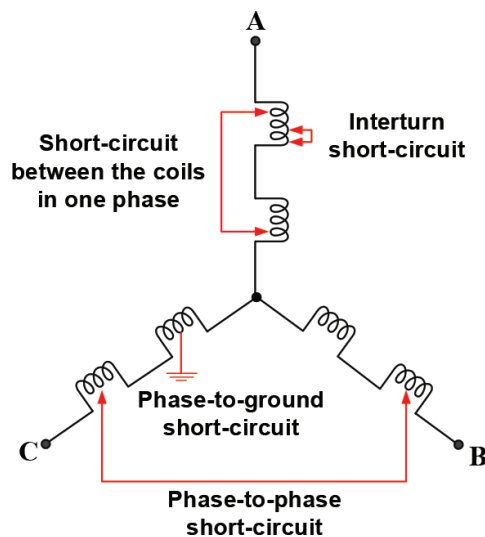


Fig. 1. PMSM stator winding short-circuit types. PMSM, permanent magnet synchronous motor.

the drive system. Considering the high percentage of stator winding failures among all PMSM faults and its very destructive nature, effective symptom extraction of this type of damage is currently one of the most important research problems. Over the years, several methods have been developed for the diagnosis of PMSM stator winding faults (Chen et al., 2019). However, new, more robust and more effective diagnostic algorithms are still being searched for.

When developing an effective diagnostic system, the basic issue is the knowledge of changes in motor operation caused by a specific fault and their subsequent monitoring based on the signals available for measurement or estimation. The stator phase current is one of the most popular signal in the diagnosis of electrical fault in PMSM (Hang et al., 2016). However, diagnostic methods that are based on other signals, such as voltage (Boileau et al. 2013), electromagnetic torque (Zhao et al., 2021), instantaneous active power (Drif and Cardoso, 2014), rotational speed (Rosero et al., 2009) and axial flux (Gurusamy et al., 2021; Skowron et al. 2021) have also been proposed in the literature.

Methods that perform analysis in the frequency domain are the most common in the field of electric motor fault diagnosis. The established and still widely used as the first diagnostic approach is the stator phase current signal analysis with fast Fourier transform (FFT) (Heno et al., 2014). The extended Park's vector approach is one of the popular improvements of the classical stator current FFT analysis-based method that has been applied in the PMSM stator winding fault diagnosis last years (Fonseca et al., 2020). Symptoms of this type of failure can also be found in the FFT spectrum of stator current symmetrical components, especially in the negative sequence component (Huang et al., 2021; Jeong et al., 2017; Pietrzak and Wolkiewicz, 2021b). The zero sequence voltage component (ZSVC) FFT analysis for the detection of PMSM stator winding faults has also been used in Fang et al. (2019). Nevertheless, the access to the neutral point of the stator winding is needed for this method. The effective on-line ITSC detection algorithm based on the ZSVC and high frequency (HF) signal injection is proposed in Zhang et al. (2021). There, ZVSC is used to detect the abnormal state of the PMSM drive, and then, the HF current signals are injected to discriminate between the ITSC and resistive unbalance fault. In Hang et al. (2022), the ITSC fault is diagnosed by ZSVC and the torque ripple caused by ITSC fault is reduced by the current injection-based fault tolerant control strategy. The spectral analysis of the reference voltages in $d-q$ frame is proposed for the on-line stator winding fault detection in PMSM drives in Ahn et al. (2019). A novel stray flux spectral analysis-based method for PMSM ITSC detection is proposed in Gurusamy et al. (2021). This method utilizes the value of the stray flux third harmonic as a fault indicator. To the more complex subgroup of the frequency domain methods belong the High Order Transforms (HOTs). HOTs have also been applied for PMSM fault diagnosis in the past. The most popular of HOTs utilized in diagnosis field are multiple signal classification (MUSIC) (Zamudio-Ramírez et al., 2020), Bispectrum (Ewert, 2020; Pietrzak and Wolkiewicz, 2022) and estimation of signal parameter by rotational invariance technique (ESPRIT) (Xu et al., 2013). However,

these methods have some significant limitations. The main limitation is the lack of information about the time of occurrence of a given frequency component and, in most cases, the need for a long measurement time to achieve high symptoms extraction effectiveness. Methods that perform time–frequency analysis do not suffer from these limitations. These methods include the application of the continuous wavelet transform (Haje Obeid et al., 2017; Park et al., 2019), Hilbert–Huang transform (Urresty et al., 2009), Wigner–Ville transform also known in the literature as Wigner–Ville distribution (Rosero et al., 2009), Gabor expansion (Dogan and Tetik, 2021) and short-time Fourier transform (STFT) (Maqsood et al., 2020). The STFT analysis has been verified in the past too in the field of PMSM faults diagnosis (Rosero et al., 2007; Zanardelli et al., 2007). Nevertheless, this research is limited to the detection of other types of damage than the stator winding fault and in a narrow range of motor operating conditions.

The processing of the diagnostic signal with the aforementioned mathematical apparatuses allows to extract the symptoms characteristic for the failure of the PMSM stator windings. The application of STFT analysis may also allow to collect data sets that contain extracted symptoms that can be successfully used to train the artificial intelligence-based stator winding fault detectors and classifiers. Moreover, it should be highlighted that fault symptoms extraction, feature processing and data collection are a crucial part of condition monitoring and predictive maintenance systems.

The contribution of this work is the application of the STFT analysis of stator phase current, stator phase current envelope and stator phase current space vector module for symptoms extraction of ITSCs in PMSM stator winding. The use of this advanced signal processing method has been compared with the classical approach – FFT. The superiority of the proposed method over this approach is highlighted. Both signal processing methods are tested for a PMSM drive system under variable load torque and rotation speed (power supply frequency).

The article is divided into six sections. Section 2 discusses the impact of ITSC on the stator current, stator current envelope and stator current space vector module waveform of PMSM drive. The theoretical basis of the STFT analysis is discussed in Section 3. In Section 4, the test stand and the methodology of experimental research are presented. In Section 5, the experimental results of FFT and STFT analyses using the aforementioned methods are demonstrated to extract the symptoms of ITSCs. The final conclusions from the conducted research are presented in Section 6.

2. Impact of ITSC on the Stator Current-Based Signals of PMSM Drive

The ITSC in the PMSM stator winding causes changes in the amplitude of the stator current and its fluctuations. However, these changes are not enough to provide effective diagnostics of this type of fault because of the impact of the load torque on stator current amplitude. To confirm it, the influence of the ITSC of the PMSM stator winding (three shorted turns) on the stator phase current waveforms during motor operation at nominal load torque ($T_L = T_N$) and nominal speed (power supply frequency $f_s = f_{sN} = 100$ Hz) is shown in Figure 2. Analysis of these waveforms shows that there is only a slight change in the current amplitude value of the faulty phase as a result of ITSC.

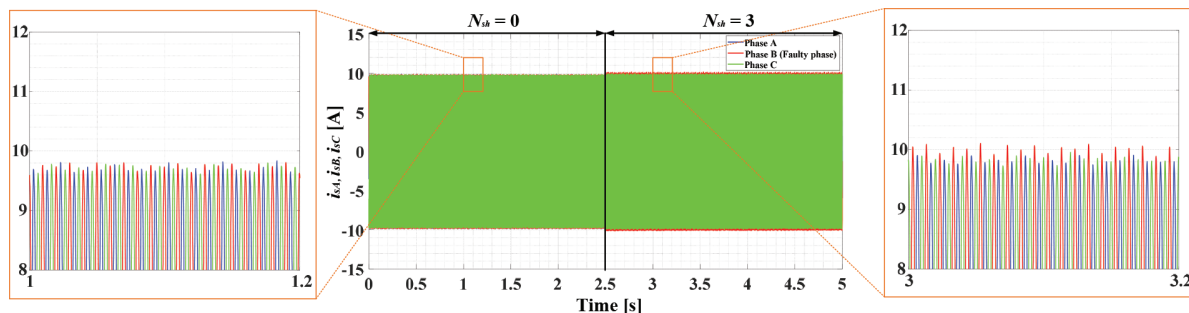


Fig. 2. The impact of the ITSC ($N_{st} = 3$) in the phase B of the PMSM stator winding on the stator current waveforms ($T_L = T_N$, $f_s = f_{sN} = 100$ Hz). ITSC, inter-turn short circuit; PMSM, permanent magnet synchronous motor.

Fluctuations in the stator phase current signal waveform can be isolated by determining the stator phase current envelope. To calculate the signal envelope, the Hilbert transform (HT) can be used. HT is determined according to Eq. (1) (Pietrzak and Wolkiewicz, 2021a):

$$i_s^H(t) = \sqrt{i_s^2(t) + H^2[i_s(t)]}, \quad (1)$$

where $H[i_s(t)]$ – HT of the phase current signal:

$$H[i_s(t)] = \frac{1}{\pi} \int_{-\infty}^{+\infty} \frac{i_s(\tau)}{t - \tau} d\tau. \quad (2)$$

The influence of the ITSC in the PMSM stator winding ($N_{sh} = 3$) on the phase current envelope signal of the faulty phase (B) during motor operation at rated operating conditions is shown in Figure 3. Analysis of these waveforms shows that there is only an insignificant change in the envelope amplitude value of the faulty phase as a result of an ITSC. As in the case of the raw stator current signal, the amplitude of its envelope also depends heavily on the load torque level, so it cannot be used for effective diagnostics without any pre-processing stage.

The next diagnostic signal that may be used to improve the effectiveness of the fault diagnosis compared to the classical analysis of the stator phase current is the stator current space vector module. The space vector module is defined in accordance with the following equation:

$$|i_s| = \sqrt{i_{s\alpha}^2 + i_{s\beta}^2}, \quad (3)$$

where $i_{s\alpha}$ and $i_{s\beta}$ are the components of the stator phase current in α - β reference frame, determined according to Eq. (4):

$$\begin{aligned} i_{s\alpha} &= \sqrt{\frac{2}{3}} \cdot \left(i_{sA} - \frac{1}{2} \cdot (i_{sB} + i_{sC}) \right), \\ i_{s\beta} &= \frac{1}{\sqrt{2}} (i_{sB} - i_{sC}), \end{aligned} \quad (4)$$

where i_{sA} , i_{sB} and i_{sC} – stator current in phases A, B and C, respectively.

The signal waveform of the stator current space vector module for an undamaged motor and after the ITSC ($N_{sh} = 3$) is shown in Figure 4. Based on this waveform, it can be concluded that the influence of the ITSC on its amplitude is slightly greater than in the case of the stator phase current signals and its envelope. Nevertheless, also in this case, the amplitude is strongly dependent on the T_L level, which is further confirmed. To extract the symptoms of the ITSCs that are independent of the motor operating conditions changes, signal pre-processing algorithms can be applied. In this work, in the pre-processing step, the application of the FFT and STFT analyses of these three signals is compared.

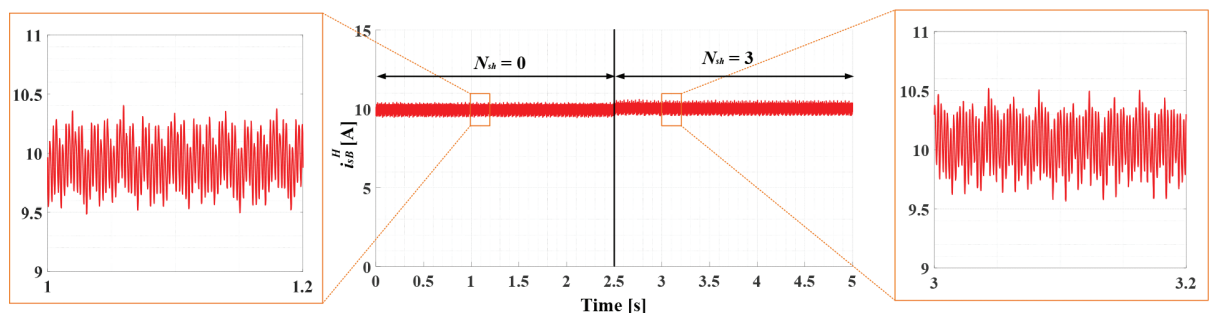


Fig. 3. The impact of the ITSC ($N_{sh} = 3$) in the PMSM stator winding on the stator current envelope waveform, Phase B ($T_L = T_N$, $f_s = f_{sN} = 100$ Hz). ITSC, inter-turn short circuit; PMSM, permanent magnet synchronous motor.

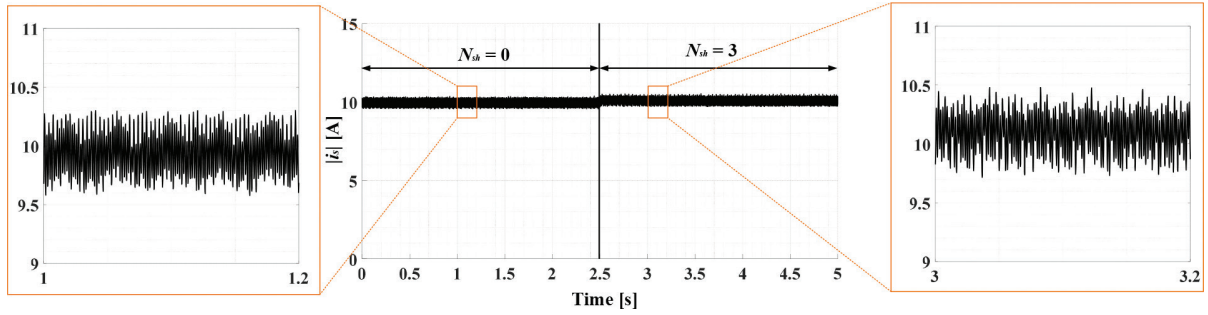


Fig. 4. The impact of the ITSC ($N_{it} = 3$) in the phase B of the PMSM stator winding on the stator current space vector module waveform ($T_L = T_N$, $f_s = f_{sN} = 100$ Hz). ITSC, inter-turn short circuit; PMSM, permanent magnet synchronous motor.

3. Short-Time Fourier Transform

The frequency domain representation of the signal provided by the FFT analysis does not contain information about the occurrence of a particular frequency over time, despite good resolution in the frequency domain (Figure 5a). Moreover, the FFT is effective only in the case of a stationary signal. In the field of electric motor fault diagnosis, it is crucial to have information about the time of the fault. Based on this information, the source of the failure can be determined. The STFT overcomes the limitations of the FFT analysis. It is an extension of the FFT for time–frequency domain analysis. This transform is also suitable for the analysis of nonstationary signals (Zanardelli et al., 2007). It provides the location in time while simultaneously capturing the frequency information. The signal segmentation (tilling) for the STFT is presented in Figure 5b. In the implementation of the STFT, a design trade-off must be made between time and frequency. A short window provides good time resolution at the expense of poor frequency resolution, whereas a long window provides good frequency resolution at the expense of reduced time resolution.

The STFT calculates the Fourier transform (FT) of a function $f(t)$ over a symmetrical and real window function $w(t)$, which is translated by time t and modulated at frequency ω . The continuous domain expression of the STFT is illustrated by Satpathi et al. (2018):

$$S(t, \omega) = \int_{-\infty}^{\infty} f(\tau) w(\tau - t) e^{-j\omega\tau} d\tau. \quad (5)$$

The magnitude of the STFT yields the spectrogram, whose amplitudes are analysed during the experiments. The spectrogram is the result of calculating the frequency spectrum of windowed frames of a compound signal. It is a three-dimensional plot of the energy of the signal frequency content as it changes over time and may be expressed by the following equation:

$$\text{spectrogram}(t, \omega) = |S(t, \omega)|^2. \quad (6)$$

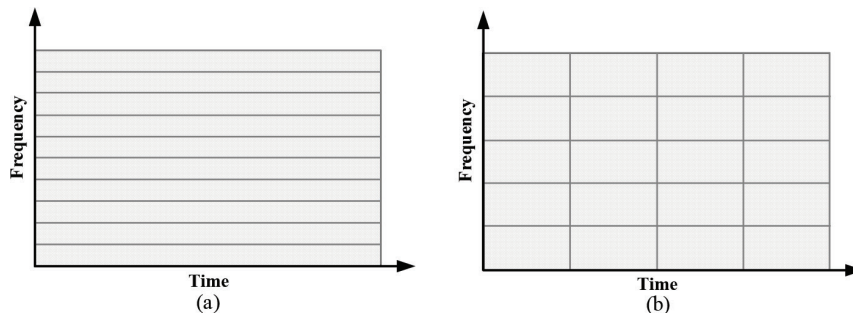


Fig. 5. (a) FFT and (b) STFT tiling. FFT, fast Fourier transform; STFT, short-time Fourier transform.

Table 1. STFT dependence parameters.

Name of the parameter	Symbol	Description
Sampling frequency	f_p	Sampling frequency affects the time and frequency resolution of the STFT output. Higher f_p results in better time and frequency resolution and vice versa. In this article, f_p of the FFT- and STFT-based analysis is set to 8,192 Hz.
Number of input samples	N_t	It is the total number of samples of the input stator phase current signal on which the windowing function is applied. For the 10 s measurement time and $f_p = 8,192$ Hz, the number of input samples is equal to 81,920.
Type of window function	$w[n]$	The most popular window functions available for performing STFT are rectangular, triangular, Hanning, Hamming and Bartlett. In this article, based on the comparisons, Hamming window function is used.
Window size	H	The window size is responsible for the STFT output resolution in time domain. The lower the size of the window, the better the resolution of the time. In this article, H is chosen to be 2,048 samples, which is equivalent to the time resolution of 0.25 s. Further, the time resolution for other H value is shown.

FFT, fast Fourier transform; STFT, short-time Fourier transform.

Table 2. Rated parameters of the tested PMSM.

Name of the parameter	Symbol	Value	Units
Power	P_N	2,500	W
Torque	T_N	16	Nm
Speed	n_N	1,500	r/min
Stator phase voltage	U_{sN}	325	V
Stator current	I_{sN}	6.6	A
Frequency	f_{sN}	100	Hz
Number of pole pairs	p_p	4	–
Number of stator turns	N_s	2×125	–

PMSM, permanent magnet synchronous motor.

In real applications, signals are sampled with a fixed sampling frequency (f_p), and discrete Fourier transform (DFT) is computed to analyse the frequency spectrum by applying the FFT algorithm. Therefore, Eq. (5) in the discrete domain is expressed as follows (Satpathi et al., 2018):

$$S_D[m, k] = \sum_{n=0}^{n=N-1} x[n]w[n-mH]e^{-j\frac{2\pi nk}{N}}, \quad (7)$$

where N – the number of FFT points, n – the time-domain input sample index, $x[n]$ – the input sample, $w[n]$ – the window function and m is its position, H – window size and k – frequency index. The STFT dependence parameters are grouped in Table 1.

4. Experimental Setup Description

The object of the experimental verification is a 2.5 kW PMSM operated in closed-loop control structure with field-oriented control (FOC). The parameters of this motor are listed in Table 2. The tested PMSM is connected via a rigid coupling to the second PMSM with a nominal power of 4.7 kW. Both motors are supplied by voltage-source inverters (VSIs). The second inverter operates in torque regulation mode. The test stand is shown in Figure 6a. The motor shown on the left side of the figure is the tested motor, while that on the right is the loading motor. The stator winding construction of the tested PMSM allows to model the ITSCs of several stator turns physically. Direct short circuits were done by connecting the taps on the terminal board with a wire. The terminal board is shown in Figure 6b. To make the tests as close to the real case as possible,

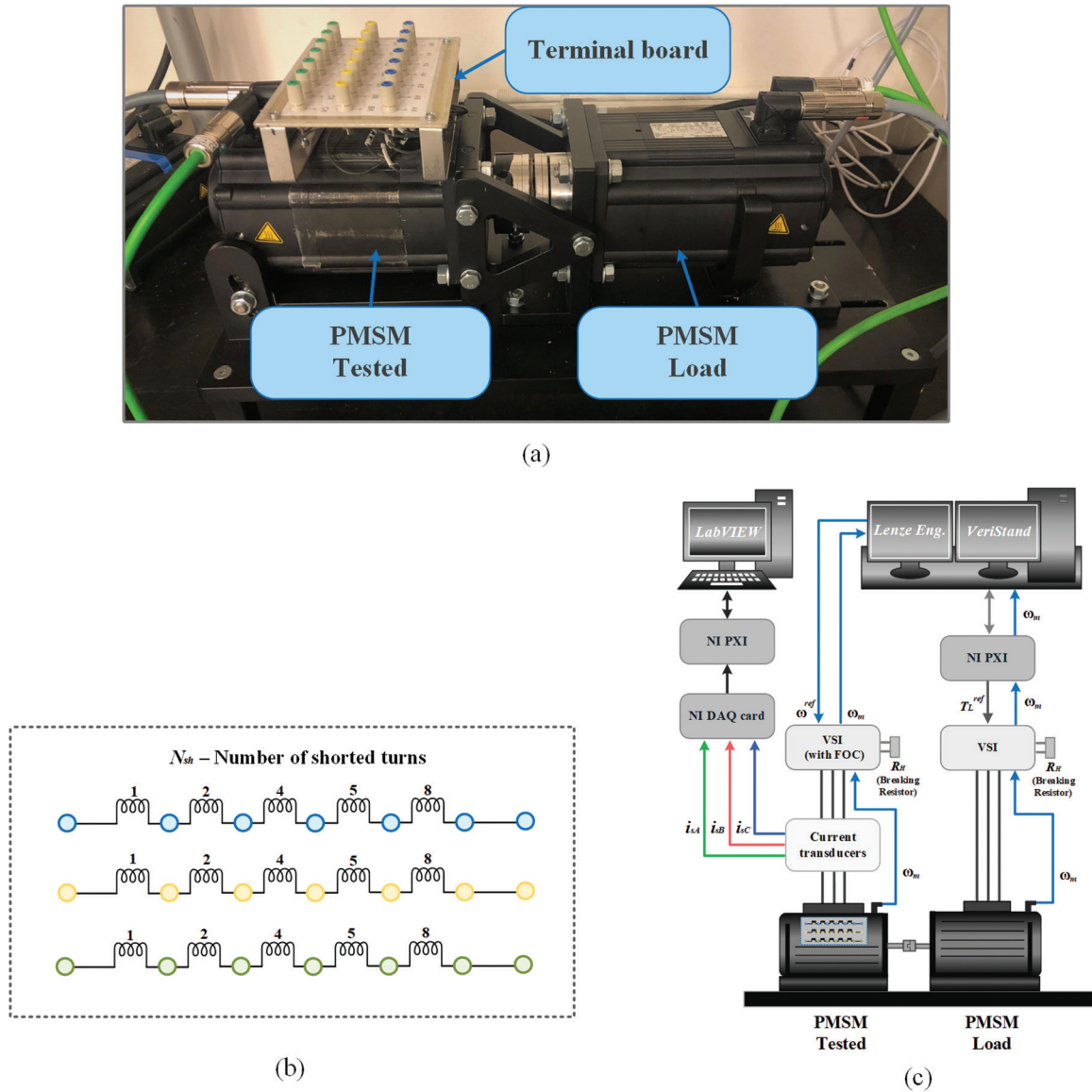


Fig. 6. (a) Real view of the experimental stand, (b) diagram of the stator winding phase terminals and (c) block diagram of the experimental setup. PMSM, permanent magnet synchronous motor.

there is no additional resistance in the short circuit. The stator phase currents are measured using LEM LA 25-NP multirange transducers. The output signals from the current transducers enter the internal eight-channel data acquisition unit DAQ NI PXI-4492 with 24-bit ADC converter. This DAQ card is placed inside the industrial PC NI PXI 1082 by National Instruments. The sampling frequency is set to 8,192 Hz. The block diagram of the experimental setup is shown in Figure 6c. The PMSM stator winding condition monitoring and fault symptom extraction algorithms are developed in LabVIEW programming environment. The signal measurement and processing application is created as a virtual measurement diagnostic tool using the graphical language ('G').

Using the described test stand, an experimental verification is conducted. Tests are carried out for various values of the load torque in the range of $0-1T_N$ with $0.2 T_N$ step and for various rotational speeds (frequency of the supply voltage, 60–100 Hz), which allowed the examination of the influence of motor operating conditions on the extracted ITSC symptoms.

5. Experimental Results

5.1. FFT analysis

5.1.1. Stator phase current

First, the FFT analysis of the stator phase current signal is carried out. In Figure 7, the stator phase current spectra (phase B) for the motor operating at nominal power supply frequency $f_s = f_{sN} = 100$ Hz and Figure 7a $T_L = 0$, Figure 7b $T_L = T_N$ for an undamaged stator winding and with three shorted turns ($N_{sh} = 3$) are shown. In these spectra, the increase in third harmonic ($3f_s$) amplitude is visible after the stator winding fault. To assess the exact impact of the ITSC on the amplitude of a given frequency component and the subsequent comparison of the increases between other diagnostic signals, the increase in the amplitude for a given N_{sh} in relation to the value for an undamaged motor is analysed:

$$A_{DIFF}(f_c) = A_{Damaged}(f_c) - A_{Undamaged}(f_c), \quad (8)$$

where f_c is the characteristic failure frequency component, $A_{Damaged}$ and $A_{Undamaged}$ are the amplitudes of f_c component for damaged and undamaged motor, respectively.

The effect of N_{sh} and T_L on the increase in the amplitude of the $3f_s$ frequency component is shown in Figure 8a, while the dependence on the f_s value is illustrated in Figure 8b. Based on the presented results, it can be concluded that the increase in amplitude of $3f_s$ caused by the stator winding fault is significant, especially in the case of the motor operating at rotation speed close to the rated value. Nevertheless, as the value of the power supply frequency f_s decreases (the lower rotation speed than the rated value), the fault sensitivity (A_{DIFF}) is much lower.

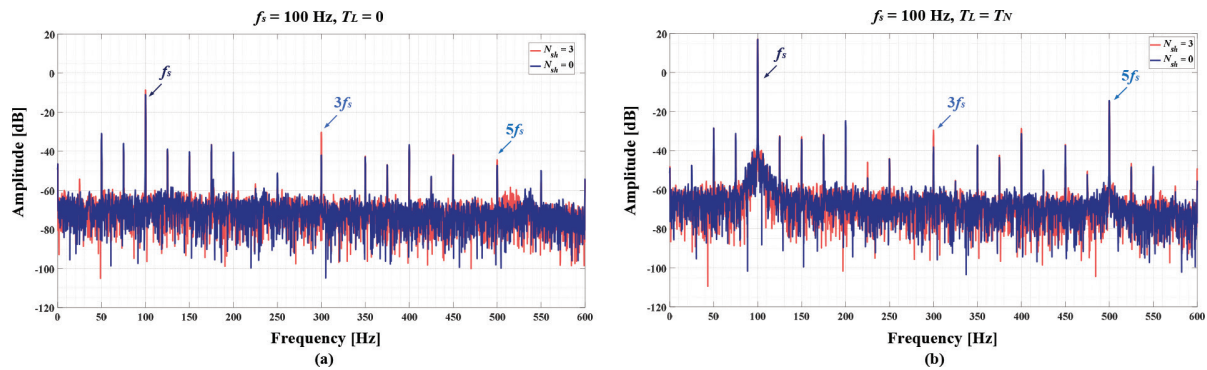


Fig. 7. The impact of shorted turns in the PMSM stator winding on the FFT spectrum of the stator phase current (a) $T_L = 0$ and (b) $T_L = T_N$ ($f_s = 100$ Hz). FFT, fast Fourier transform; PMSM, permanent magnet synchronous motor.

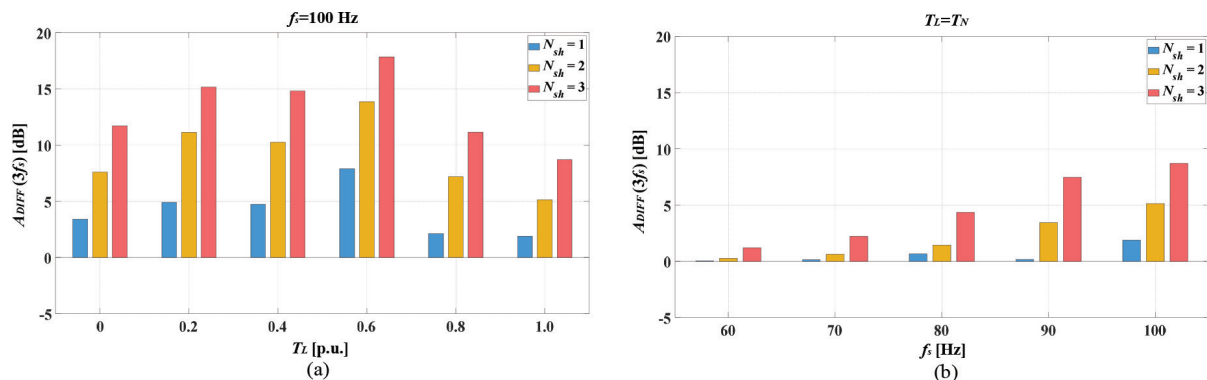


Fig. 8. The impact of N_{sh} on the PMSM stator winding and (a) T_L and (b) f_s values on the increase in amplitude of $3f_s$ frequency component in the stator current FFT spectrum. FFT, fast Fourier transform; PMSM, permanent magnet synchronous motor.

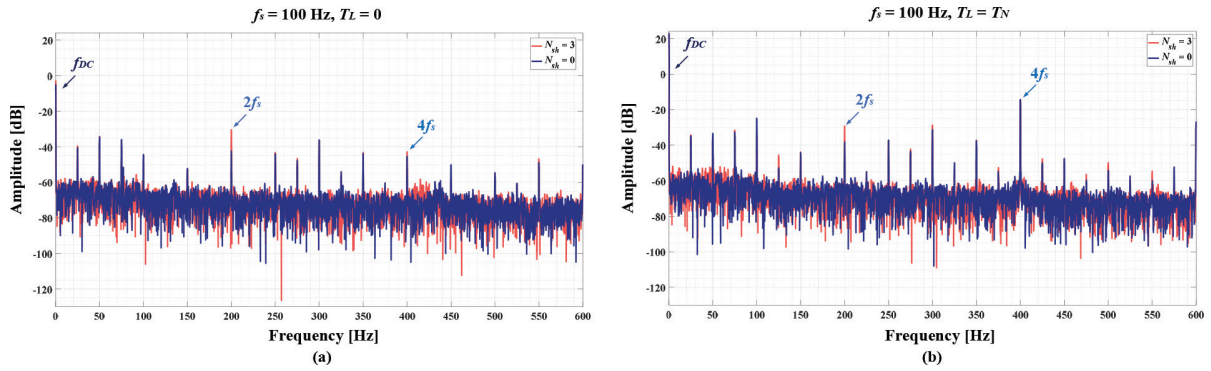


Fig. 9. The impact of shorted turns in the PMSM stator winding on the FFT spectrum of the stator phase current envelope (a) $T_L = 0$ and (b) $T_L = T_N$ ($f_s = 100$ Hz). FFT, fast Fourier transform; PMSM, permanent magnet synchronous motor.

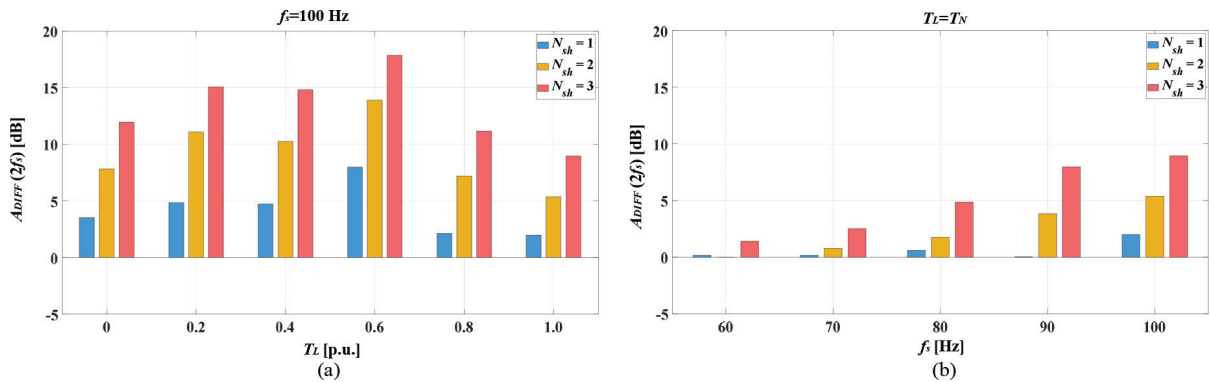


Fig. 10. The impact of N_{sh} on the PMSM stator winding and (a) T_L and (b) f_s values on the increase in amplitude of $2f_s$ frequency component in the stator current envelope FFT spectrum. FFT, fast Fourier transform; PMSM, permanent magnet synchronous motor.

5.1.2. Stator phase current envelope

In the next step, the application of the stator phase current envelope signal FFT analysis to the ITSC detection is verified. The FFT spectra of the stator phase current envelope for the motor operating with $f_s = f_{sN} = 100$ Hz and (a) $T_L = 0$, (b) $T_L = T_N$ for an undamaged stator winding and N_{sh} are presented in Figure 9. In this case, an increase in the amplitude of the second harmonic ($2f_s$) is visible after the stator winding fault. The effect of N_{sh} and T_L on the increase of $2f_s$ amplitude after ITSC is shown in Figure 10a. The influence of the power supply frequency value f_s is shown in Figure 10b. Based on the bar charts presented in these figures, it can be concluded that the increase in amplitude of $2f_s$ caused by the stator winding fault is significant. However, as in the case of stator phase current spectral analysis, when the value of the power supply frequency f_s decreases, the fault sensitivity of this component to damage is also lower.

5.1.3. Stator phase current space vector module

Figure 11 shows the spectra of the stator phase current space vector module for the motor operating under the same conditions as for the stator current and the stator current envelope signal. The stator winding fault results in the significant increase in the amplitude of the $2f_s$ component. The influence of stator winding fault and T_L changes on the $2f_s$ amplitude difference compared to the undamaged motor after the ITSC is shown in Figure 12a. The effect of the frequency of the supply voltage f_s is shown in Figure 12b. The amplitude of the $2f_s$ component is very sensitive to the stator winding faults. The values of increases are higher compared to the results described previously, especially when the motor is operating at rated condition. Nevertheless, the T_L value has an impact on the increase in amplitude as a result of ITSC, which is especially visible for $T_L = 0.6T_N$ and $T_L = 0.8T_N$.

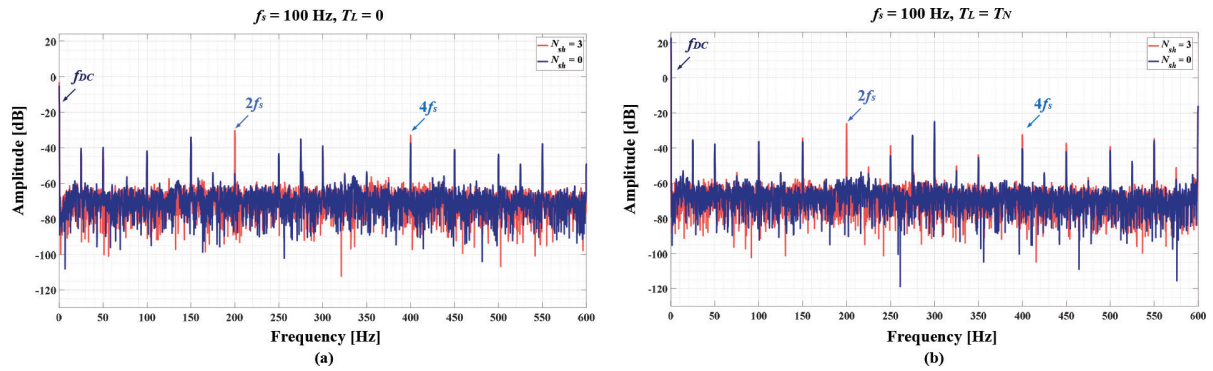


Fig. 11. The impact of shorted turns in the PMSM stator winding on the FFT spectrum of the stator phase current space vector module (a) $T_L = 0$ and (b) $T_L = T_N$ ($f_s = 100$ Hz). FFT, fast Fourier transform; PMSM, permanent magnet synchronous motor.

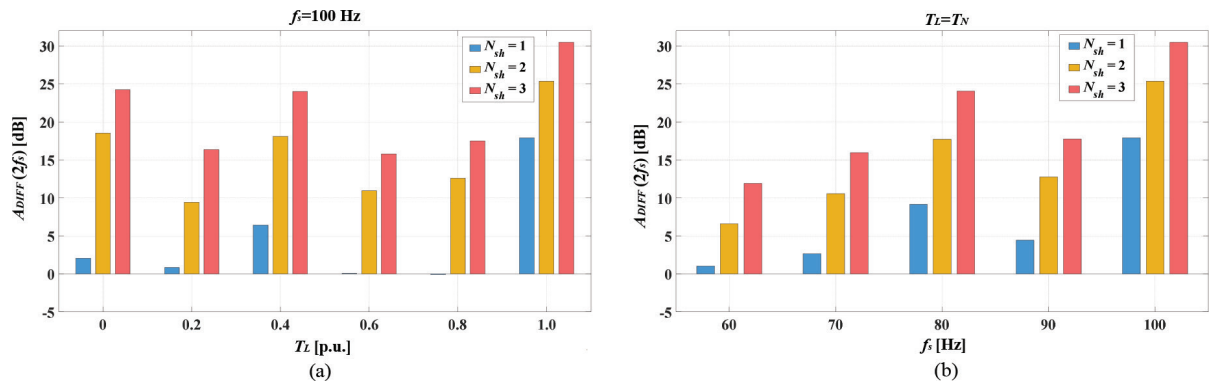


Fig. 12. The impact of N_{sh} on the PMSM stator winding and (a) T_L and (b) f_s values on the increase in amplitude of $2f_s$ frequency component in the FFT spectrum of the stator phase current space vector module. FFT, fast Fourier transform; PMSM, permanent magnet synchronous motor.

5.1.4. Results comparison

The comparison of the results presented in the previous subsections has to be made to select the most suitable signal for the diagnosis of PMSM stator winding failure based on the FFT analysis. Following to this, the amplitude increase of the characteristic failure components as a results of the ITSC for each of verified diagnostic signals is presented in Figure 13. The comparison is conducted for different values of the load torque T_L (Figure 13a) and power supply frequency f_s (Figure 13b). Based on this comparison, it can be concluded that the sensitivity to the ITSC for the $3f_s$ component in the stator phase current FFT spectrum and $2f_s$ component in the stator phase current envelope FFT spectrum is very similar. A much larger increase in the value of the amplitude as a result of the stator winding fault is visible for the $2f_s$ component in the spectrum of the stator phase current space vector module. It is also visible at low frequencies of the power supply voltage. Thus, it can be concluded that the most sensitive symptom is the amplitude change of this component. Nevertheless, it should be remembered that to calculate the module of the stator phase current space vector, it is necessary to have information about the current in all three phases.

5.2. STFT analysis

5.2.1. Introduction

As previously mentioned, proper selection of the STFT window width H is essential to provide efficient fault symptoms extraction. Nevertheless, there is no single method for selecting this value. The proper H value depends on the nature of the analysed signal, measurement parameters and the specific application. The STFT spectrograms of a 10-s stator current signal ($t_m = 10$ s) sampled with frequency $f_p = 8,196$ Hz and different H are shown in Figure 14. As can be seen, depending on the window width, good resolution is achieved in the time or frequency domain. The smaller the window width, the better resolution in the time domain. As shown in Figure 15, for $H = 2,048$, the resolution is 0.25 s in the time domain and 4 Hz in the frequency, for $H = 4,096 - 0.5$ s and 2 Hz, $H = 8,196 - 1$ s

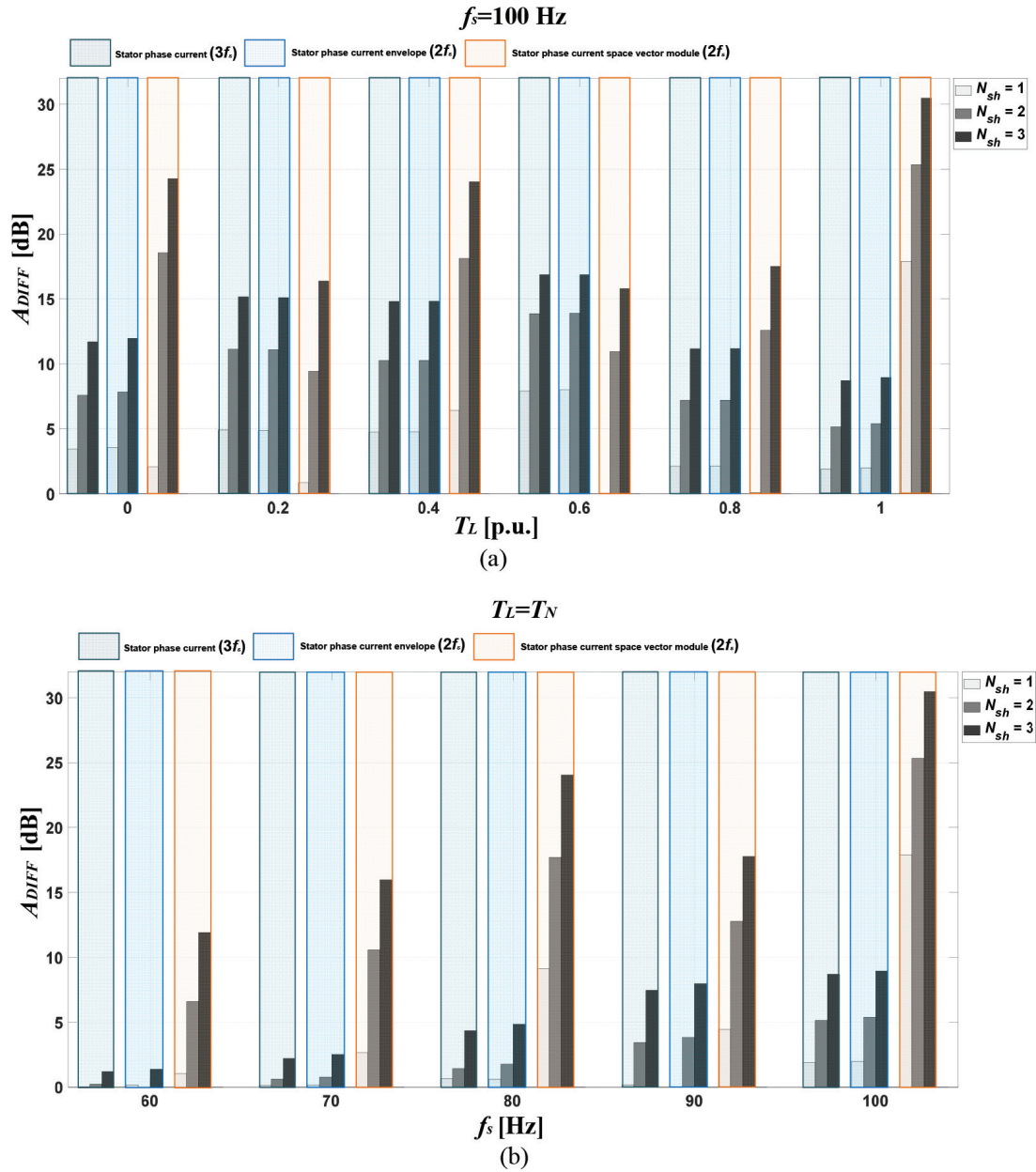


Fig. 13. The comparison of the FFT analysis results presented in the previous subsections for different value of (a) T_L and (b) f_s . FFT, fast Fourier transform.

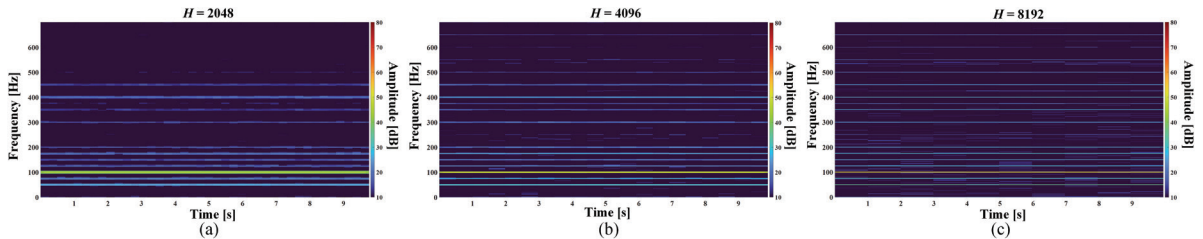


Fig. 14. Stator phase current STFT spectrograms for different window width values (a) $H = 2,048$, (b) $H = 4,096$ and (c) $H = 8,192$ ($f_s = f_{sN} = 100 \text{ Hz}$, $T_L = 0$). STFT, short-time Fourier transform.

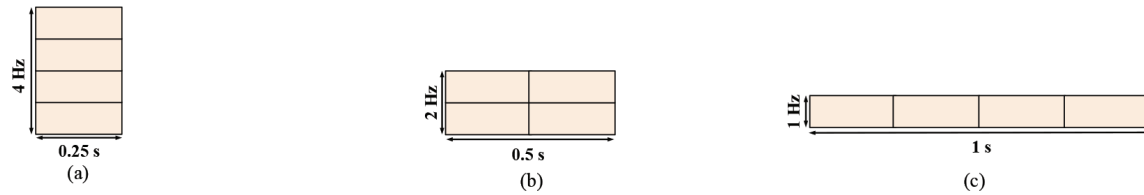


Fig. 15. The resolution obtained in the time and frequency domain for different window width values (a) $H = 2,048$, (b) $H = 4,096$ and (c) $H = 8,192$ ($f_p = 8,196$ Hz, $t_m = 10$ s).

and 1 Hz. The STFT spectrograms of the stator phase current clearly show the influence of the window width on the resolution in a given domain. The spectrograms also show that apart from the dominant component corresponding to the frequency of the supply voltage ($f_s = 100$ Hz), the other components with less significant amplitudes are visible, which is typical for a PMSM motor powered by VSI.

5.2.2. Stator phase current

As in the case of the FFT analysis, also for the STFT, the effectiveness in the extraction of PMSM winding fault symptoms is verified by analysing the stator phase current signal, its envelope and the stator phase current module. Nevertheless, taking into account the main advantage of STFT, that is the possibility of determining the fault time, the analysis is divided into steady short circuits (short circuit of a given N_{sh} for 10 s) and momentary short-circuits during on-line operation of the drive system (short circuits of a given N_{sh} for ≈ 1 s) for various motor operation conditions. To compare the efficiency of ITSC symptom extraction with the classic method based on FFT analysis and to assess the intensity of changes caused by faults, the mean values from 10 s are adopted as the value of the fault components for comparison. It can be defined with the following equation:

$$f_{cAMPavg} = \frac{1}{N-1} \sum_{n=1}^N f_{cAMP}(n), \quad (9)$$

where N_t – number of samples corresponding to the measurement time t_m ($N_t = 81,960$ for $f_p = 8,196$ Hz and $t_m = 10$ s), $f_{cAMP}(n)$ – the amplitude of the frequency component characteristic for the ITSC for the n sample.

To assess the exact impact of the damage on the amplitude of a given frequency component, the average increase in the amplitude for a given N_{sh} in relation to the value for an undamaged winding is analysed in the same manner as for the FFT results. The STFT spectrograms of the stator current signal for an undamaged PMSM and with three shorted turns in the stator winding are presented in Figure 16 ($f_s = f_{sN} = 100$ Hz, $T_L = T_N$, $H = 2,048$). The figures show a considerable increase in the amplitude value of the frequency corresponding to the third harmonic ($3f_s = 300$ Hz). Moreover, a significant effect of the change in load torque on the amplitudes of the first and fifth harmonics is visible. The other harmonics with lower amplitude that are not susceptible to ITSCs are also noticed. The effect of N_{sh} and T_L on the increase in the amplitude of $3f_s$ frequency on the stator phase current STFT spectrogram is shown in Figure 17a, while the dependence on the f_s value is illustrated in Figure 17b. It can be deduced that the increase in amplitude is more robust to changes in load torque than for FFT analysis. Moreover, this component is more sensitive to the ITSC at lower frequencies (60–90) Hz in the very early stage of the damage ($N_{sh} = 1$) compared to the FFT-based method.

5.2.3. Stator phase current envelope

Second, the STFT analysis of the stator phase current envelope is carried out. The STFT spectrograms of this signal for an undamaged PMSM and with three shorted turns are presented in Figure 18 ($f_s = f_{sN}$, $T_L = T_N$). In this case, the increase in the amplitude value of the $2f_s$ frequency component after the ITSC is visible. The amplitudes of the f_{DC} , f_s and $4f_s$ frequency components are significantly affected by the load torque changes and are not sensitive to the ITSC. The influence of the N_{sh} and T_L on the increase in the amplitude of the $2f_s$ frequency component is shown in Figure 19a, while the effect of the f_s value is presented in Figure 19b. In this case, the results are very similar to the stator phase current STFT analysis. The ITSC fault sensitivity is greater in the early stage of the failure compared to the FFT stator current envelope.

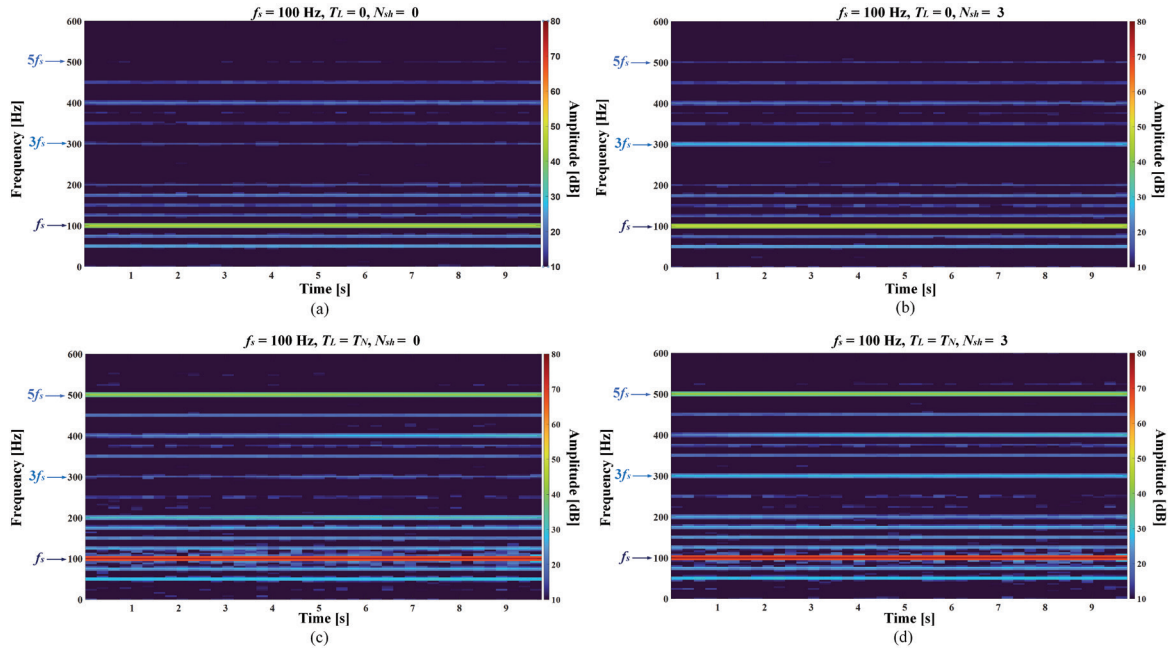


Fig. 16. Stator current STFT spectrograms for undamaged stator winding (a) $T_L = 0$, (c) $T_L = T_N$ and three shorted turns (b) $T_L = 0$, (d) $T_L = T_N$ ($f_s = 100$ Hz). STFT, short-time Fourier transform.

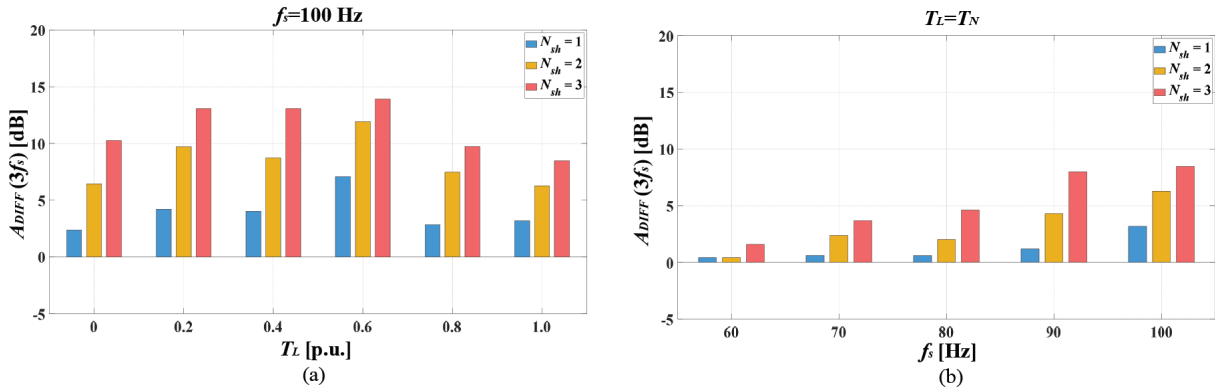


Fig. 17. The impact of N_{sh} on the PMSM stator winding and (a) T_L and (b) f_s values on the increase in the amplitude of $3f_s$ frequency component in the stator phase current STFT spectrogram. STFT, short-time Fourier transform; PMSM, permanent magnet synchronous motor.

5.2.4. Stator phase current space vector module

The STFT spectrograms of the stator phase current space vector module signal for an undamaged PMSM and with three shorted turns in the stator winding are presented in Figure 20 ($f_s = f_{sN} = 100$ Hz, $T_L = T_N$, $H = 2,048$). In this case, as in the case of the stator phase current envelope, the increase in the amplitude value of the $2f_s$ component can be observed. However, the increase is much higher compared to the previously analysed signals. The effect of N_{sh} and T_L on the increase in the amplitude of the $2f_s$ frequency on the STFT spectrogram of the stator phase current space vector module is shown in Figure 21a, while the dependence on the f_s value is illustrated in Figure 21b. It can be deduced that the increase in amplitude is more robust to changes in load torque than for FFT analysis. Moreover, this component is more sensitive to the ITSC at lower frequencies (60–90) Hz in the very early stage of the damage ($N_{sh} = 1$) compared to the previously conducted analysis.

5.2.5. Testing of the proposed fault symptoms of ITSCs in on-line operation of the drive system

To emphasize the main advantage of the STFT analysis – the possibility of on-line tracking of the faulty harmonics, keeping information about the time of frequency occurrence, the effectiveness of the proposed method of extracting

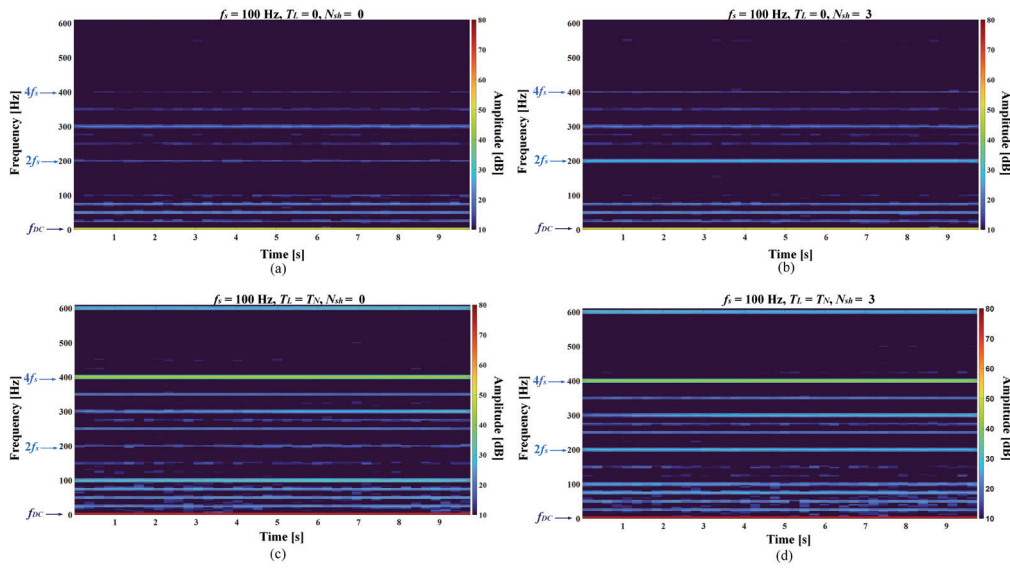


Fig. 18. STFT spectrograms of the stator current envelope for undamaged stator winding (a) $T_L = 0$, (c) $T_L = T_N$ and three shorted turns (b) $T_L = 0$, (d) $T_L = T_N$ ($f_s = 100$ Hz). STFT, short-time Fourier transform.

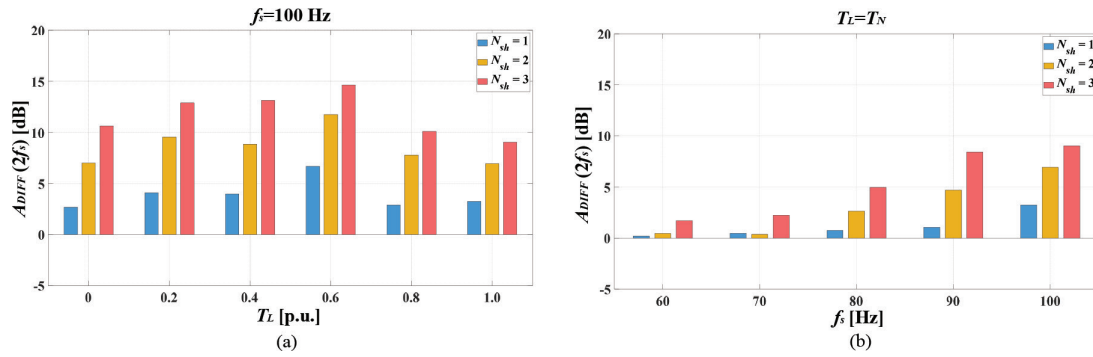


Fig. 19. The impact of N_{sh} on the PMSM stator winding and (a) T_L and (b) f_s values on the increase in the amplitude of $2f_s$ frequency component in the STFT spectrogram of the stator phase current envelope. STFT, short-time Fourier transform; PMSM, permanent magnet synchronous motor.

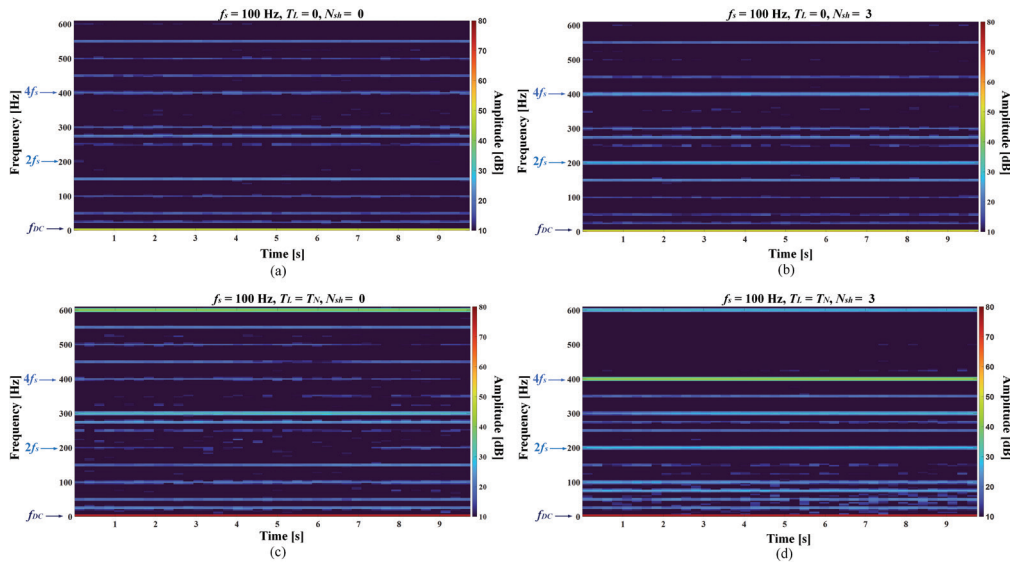


Fig. 20. STFT spectrograms of the stator current space vector module for undamaged stator winding (a) $T_L = 0$, (c) $T_L = T_N$ and three shorted turns (b) $T_L = 0$, (d) $T_L = T_N$ ($f_s = 100$ Hz). STFT, short-time Fourier transform.

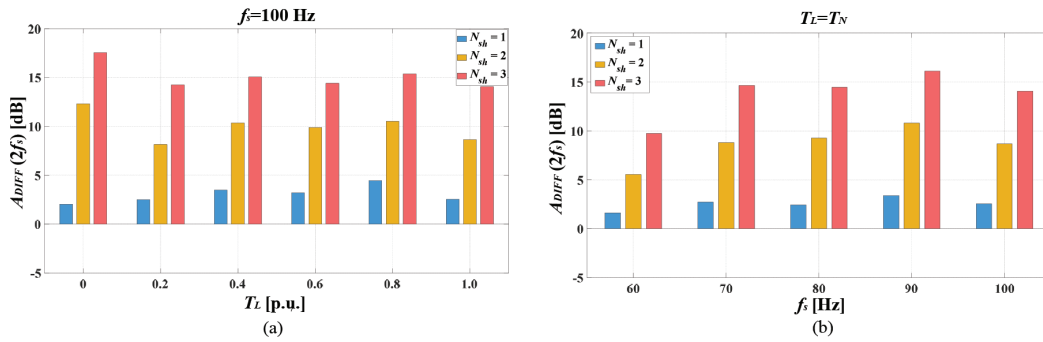


Fig. 21. The impact of N_{sp} on the PMSM stator winding and (a) T_L and (b) f_s values on the increase in the amplitude of $2f_s$ frequency component in the STFT spectrogram of the stator phase current space vector module. STFT, short-time Fourier transform; PMSM, permanent magnet synchronous motor.

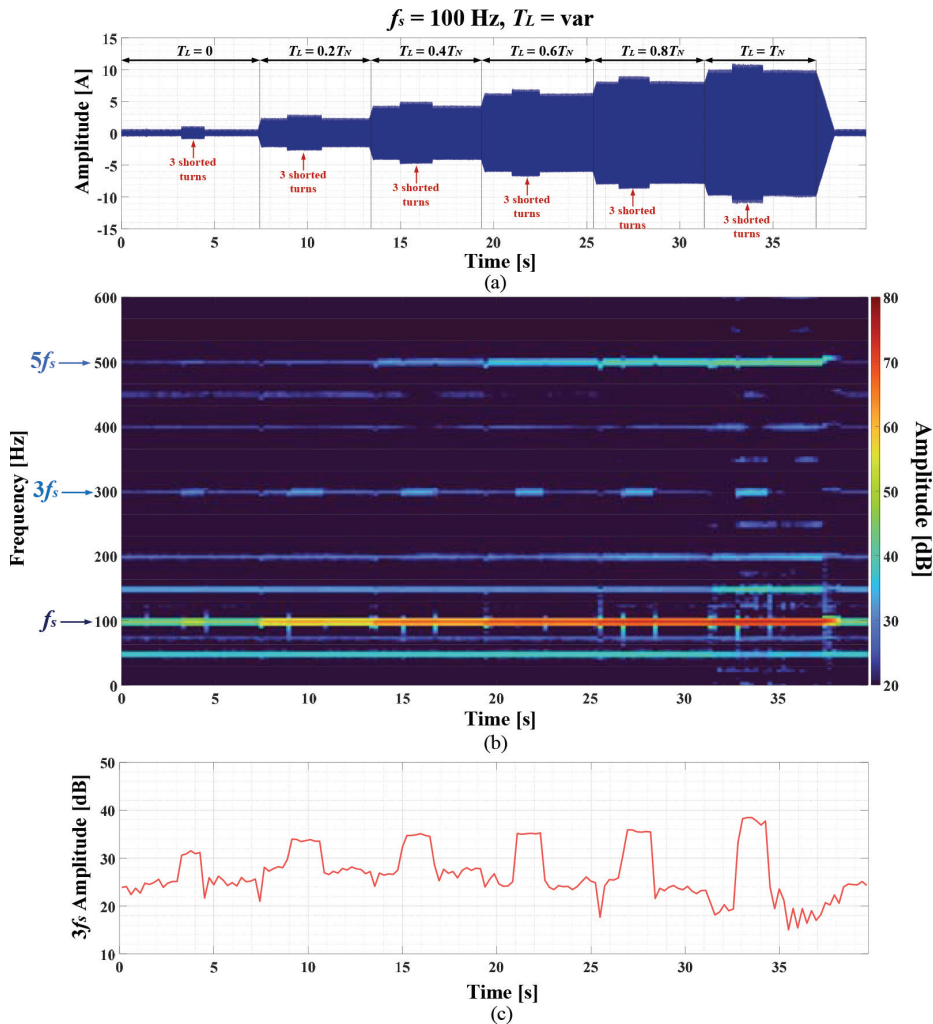


Fig. 22. The stator phase current (a) waveform, (b) STFT spectrogram and (c) $3f_s$ amplitude changes during the on-line operation of the drive system and cyclic instantaneous short circuiting of three turns at variable load torque. STFT, short-time Fourier transform.

symptoms for instantaneous short circuits during on-line operation of the drive system and changing T_L is verified. In Figure 22, the stator phase current signal waveform (Figure 22a), STFT spectrogram (Figure 22b) and value changes of the harmonic amplitude of the $3f_s$ frequency component during the on-line operation (Figure 22c) are

presented. In this scenario, T_L value is increased with $0.2T_L$ step and for each value, the momentary ITSC is performed ($N_{sh} = 3$).

Based on the analysis of these results, it can be seen that the use of the stator current STFT allows to track of changes in the amplitudes of the frequency components during on-line operation, also in the case of changing (transient) operation conditions. It is clearly visible which harmonics are sensitive to the ITSC ($3f_s$). The spectrogram also shows that the amplitudes of the f_s and $5f_s$ components increase with increasing T_L . Due to the fact that spectrograms add time to the analysis of FFT allowing the localization of both time and frequency, this can help locate the source of the fault by analysing changes in other process parameters prior to failure.

Figure 23 shows the stator phase current envelope waveform (Figure 23a), STFT spectrogram (Figure 23b) and value changes of the $2f_s$ frequency component (Figure 23c) during the on-line operation and momentary short

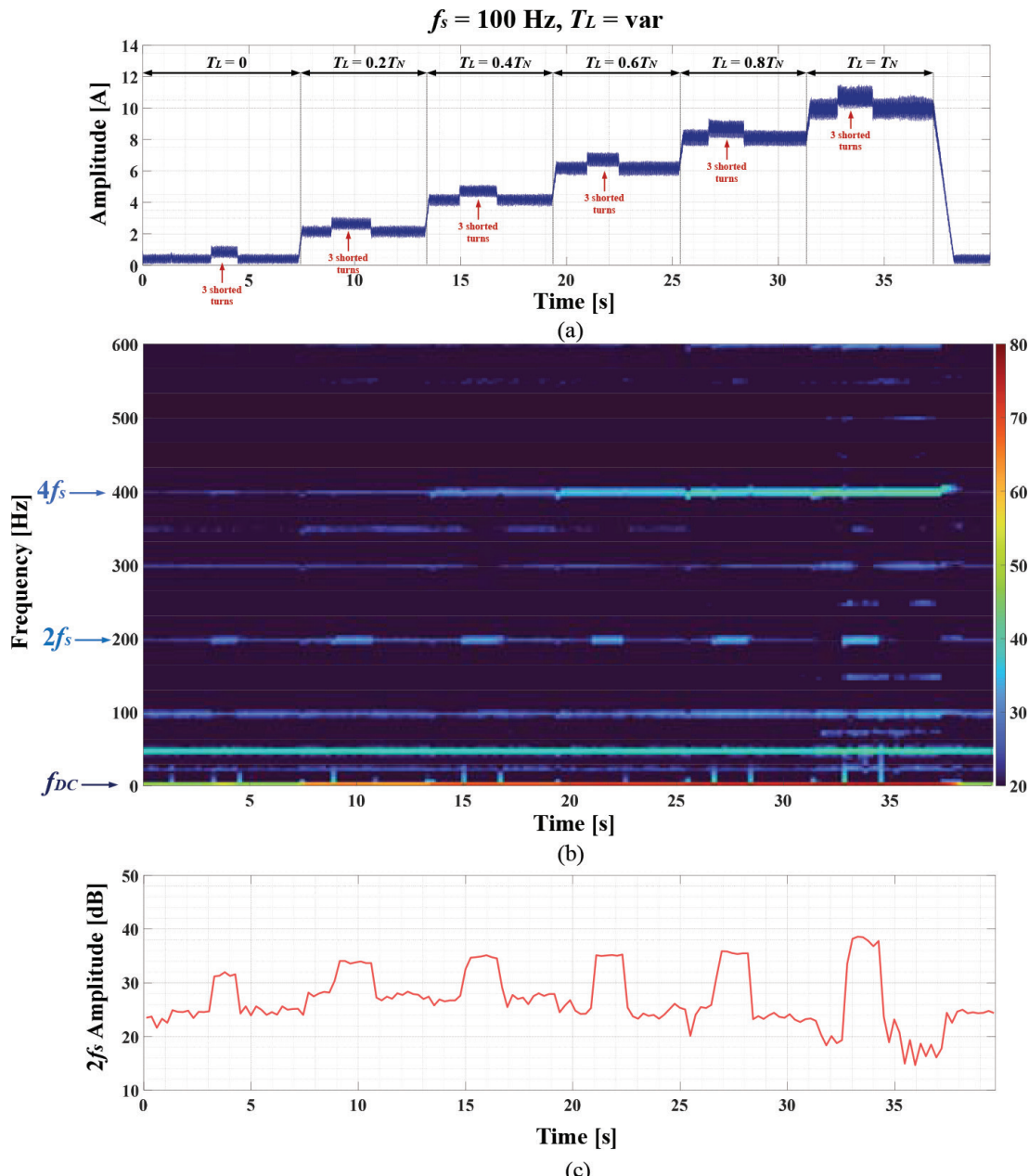


Fig. 23. The stator phase current envelope (a) waveform, (b) STFT spectrogram and (c) $2f_s$ amplitude changes during the on-line operation of the drive system and cyclic instantaneous short circuiting of three turns at variable load torque. STFT, short-time Fourier transform.

circuit of the three turns. The results confirmed the significant impact of the T_L level on the amplitude of the stator phase current signal envelope. In this case, the on-line monitoring of the $2f_s$ component may allow for the detection of the ITSC in the PMSM stator winding. It is also visible, that the value of the amplitude of f_{dc} and $4f_s$ frequency components strongly depends on the load torque.

In Figure 24, the stator phase current space vector module waveform (Figure 24a), STFT spectrogram (Figure 24b) and value changes of the $2f_s$ frequency component during the on-line operation and momentary short circuit of the three turns are presented. Based on the analysis of results presented in this figure, it can be concluded that same as in the case of the stator phase current envelope, after the ITSC in the stator winding the increase in the amplitude of the $2f_s$ frequency component is significant, which is especially visible in Figure 24c. The $2f_s$ amplitude values for an undamaged motor and for a PMSM with damaged stator winding differ significantly, more than in the case of the analysis of previous signals, which makes this component a very good fault indicator.

Based on the results analysis, it can be concluded that the application of STFT analysis may allow to collect data sets which contain extracted symptoms that can be successfully used to train the artificial intelligence-based fault

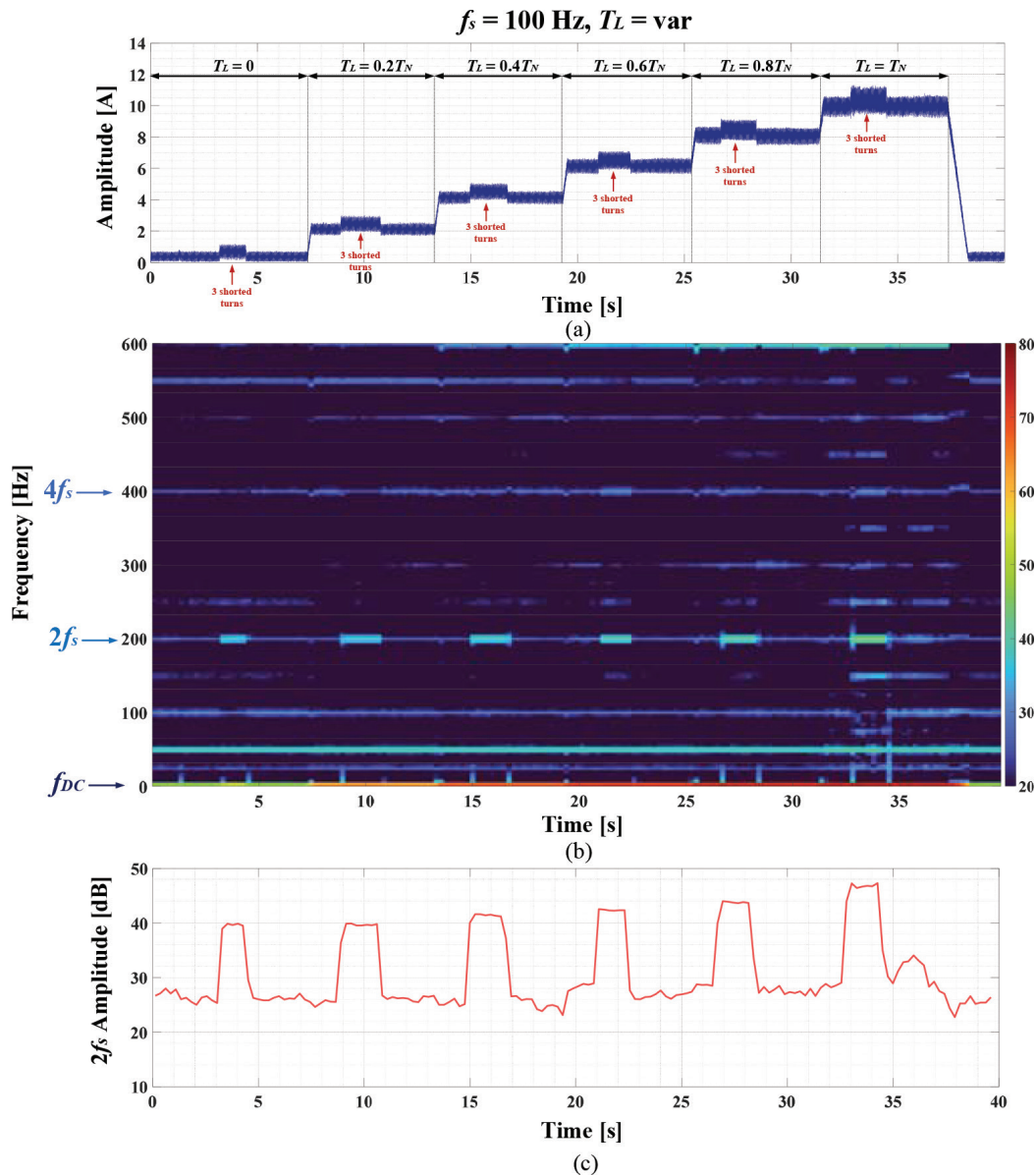


Fig. 24. The stator phase current space vector module (a) waveform, (b) STFT spectrogram and (c) $2f_s$ amplitude changes during the on-line operation of the drive system and cyclic instantaneous short circuiting of three turns at variable load torque. STFT, short-time Fourier transform.

detectors and classifiers. The training of such models for different operating conditions of the motor and different states of the stator winding may allow for the automation of the detection process without the need to define a single threshold value, which would be complicated considering the wide range of operating conditions under which modern drive systems operate. As input of the models, the raw values of the characteristic failure frequencies or spectrograms images may be utilized. The comparison of the results obtained after processing the stator phase current, stator phase current envelope and stator phase current space vector module during the steady short circuits and online operation of the drive system is discussed in the next subsection.

5.2.6. Results comparison

The amplitude increase of the characteristic failure components as a result of the ITSC for each of the verified diagnostic signals and for the first stage of the research (steady short circuits – short-circuit of a given N_{sh} for 10 s) is presented in Figure 25. The comparison is conducted for different value of the load torque T_L (Figure 25a)

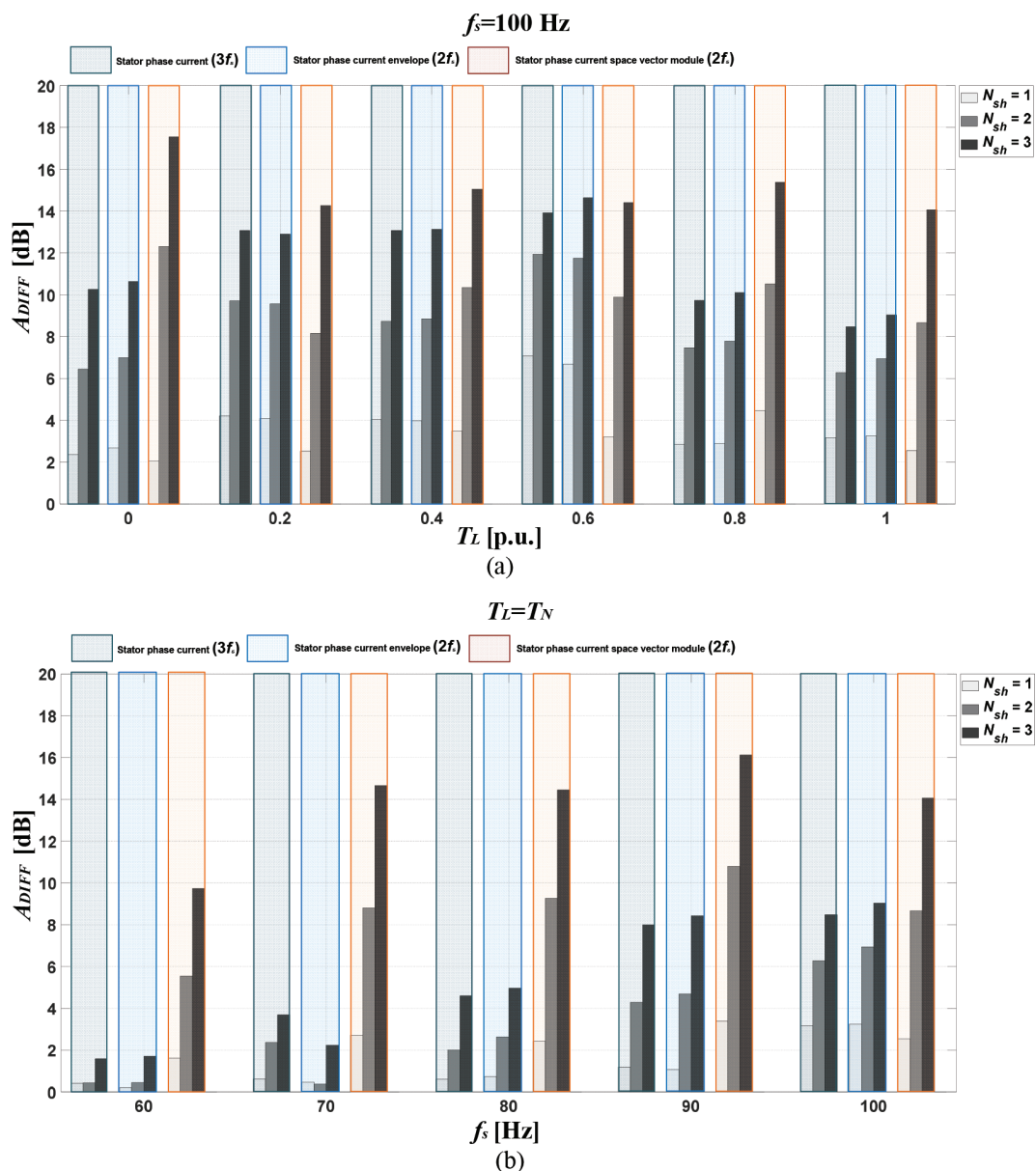


Fig. 25. The comparison of the STFT analysis results presented in the previous subsections for different values of (a) T_L and (b) f_s . STFT, short-time Fourier transform.

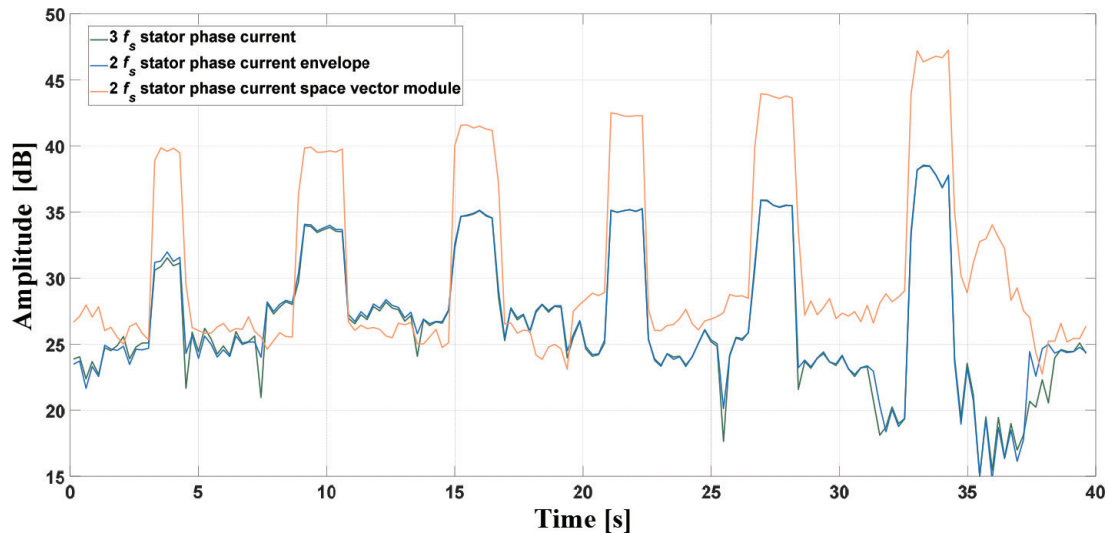


Fig. 26. The amplitude changes of the characteristic failure frequencies during the on-line operation of the drive system and cyclic instantaneous short circuiting of three turns at variable load torque.

and power supply frequency f_s (Figure 25b). From this comparison, it follows that the sensitivity to the ITSC for the $3f_s$ component in the stator phase current STFT spectrogram and $2f_s$ component in the stator phase current envelope STFT spectrogram is comparable. Nevertheless, again a much significant increase in the value of the amplitude as a result of the stator winding fault is visible for the $2f_s$ component in the spectrogram of the stator phase current space vector module. Most importantly, it is also visible at low frequencies of the power supply voltage (rotation speed). Thus, it can be concluded that the most suitable symptom is the amplitude change of this component. The amplitude changes of the characteristic failure frequencies – $3f_s$ in the stator phase current spectrogram and $2f_s$ in the stator phase current envelope and space vector module spectrogram – during the on-line operation of the drive system and cyclic instantaneous short circuiting of three turns at variable load torque are presented in Figure 26. This confirms the greatest sensitivity of symptoms appearing in the stator current space vector module; however, based on the stator phase current signal and its envelope, it is also possible to conduct effective diagnostics.

6. Conclusions

This article has addressed the issue of the PMSM stator winding fault diagnosis. The two signal processing methods: the well-known FFT analysis and the STFT analysis are proposed to the ITSCs symptoms extraction. The analysis has not only been performed for the stator phase current signal but has also been extended to the stator phase current and the stator phase current space vector module, which is a notable contribution to the topic of PMSM electrical failure detection.

The presented results of the experimental research confirm the effectiveness of the application of the STFT analysis of the stator phase current, stator phase current envelope and stator phase current space vector module to the symptom extraction of the ITSCs in the PMSM stator winding. Unlike the FFT analysis, which is also useful for the extraction of these symptoms, the STFT-based approach allows to determine the time of the failure occurrence and to track harmonics amplitudes during the on-line operation of the drive system, also in transient conditions – changing motor operating conditions. This is an important property that makes the STFT approach better than classic FFT. This method also provides higher sensitivity to failure when the rotation speed (power supply frequency) is significantly lower than the rated value at an early stage. Moreover, STFT provides greater robustness to changes in load torque compared to the FFT analysis.

Based on the thorough analysis of the results, the most promising (most sensitive to the fault in a wide range of motor operating conditions) is the STFT analysis of the stator current space vector module. The results presented in this article fill the lack of work in the field of motor diagnostics dealing with STFT analysis for the detection of

stator winding faults. In addition, these results can be useful in the development of automatic diagnostic systems, including those based on artificial intelligence, whose basis is an appropriate selection of features characteristic for failure. As the input data of such fault detectors models, the amplitudes of failure frequencies indicated as the most ITSC fault-sensitive may be used. Training dataset can be collected through experimental research for various motor operating conditions and stator winding states, as has been presented in this article.

Further research will focus on the development of PMSM automatic real-time stator winding condition monitoring and fault diagnosis system. Nevertheless, for such purposes, the profound influence of measurement accuracy (e.g. sampling frequency, measurement resolution, current sensor noise) on the diagnostic system has to be also considered.

Acknowledgements

This research was funded by the National Science Center Poland under Grant No. 2017/27/B/ST7/00816.

References

- Ahn, G., Lee, J., Park, C.H., Youn, M. and Youn, B.D. (2019). Inter-turn short circuit fault detection in permanent magnet synchronous motors based on reference voltage. In: *Proceedings of 2019 IEEE 12th International Symposium on Diagnostics for Electrical Machines, Power Electronics and Drives (SDEMPED)*, Toulouse, France, pp. 245–2450.
- Boileau, T., Leboeuf, N., Nahid-Mobarakeh, B. and Meibody-Tabar, F. (2013). Synchronous Demodulation of Control Voltages for Stator Interturn Fault Detection in PMSM. *IEEE Transactions on Power Electronics*, 28(12), pp. 5647–5654.
- Chen, Y., Liang, S., Li, W., Liang, H. and Wang, C. (2019). Faults and Diagnosis Methods of Permanent Magnet Synchronous Motors: A Review. *Applied Sciences*, 9(10), p. 2116.
- Dogan, Z. and Tetik, K. (2021). Diagnosis of Inter-Turn Faults Based on Fault Harmonic Component Tracking in LSPMSMs Working Under Nonstationary Conditions. *IEEE Access*, 9, pp. 92101–92112.
- Drif, M. and Cardoso, A. J. M. (2014). Stator Fault Diagnostics in Squirrel Cage Three-Phase Induction Motor Drives Using the Instantaneous Active and Reactive Power Signature Analyses. *IEEE Transactions on Industrial Informatics*, 10(2), pp. 1348–1360.
- Ewert, P. (2020). The Application of the Bispectrum Analysis to Detect the Rotor Unbalance of the Induction Motor Supplied by the Mains and Frequency Converter. *Energies*, 13(11), p. 3009.
- Fang, J., Sun, Y., Wang, Y., Wei, B. and Hang, J. (2019). Improved ZSVC-Based Fault Detection Technique for Incipient Stage Inter-Turn Fault in PMSM. *IET Electric Power Applications*, 13(12), pp. 2015–2026.
- Fonseca, D. S. B., Santos, C. M. C. and Cardoso, A. J. M. (2020). Stator Faults Modeling and Diagnostics of Line-Start Permanent Magnet Synchronous Motors. *IEEE Transactions on Industrial Applications*, 56(3), pp. 2590–2599.
- Gurusamy, V., Bostanci, E., Li, C., Qi, Y. and Akin, B. (2021). A Stray Magnetic Flux-Based Robust Diagnosis Method for Detection and Location of Interturn Short Circuit Fault in PMSM. *IEEE Transactions on Instrumentation and Measurement*, 70, pp. 1–11.
- Haje Obeid, N., Battiston, A., Boileau, T. and Nahid-Mobarakeh, B. (2017). Early Intermittent Interturn Fault Detection and Localization for a Permanent Magnet Synchronous Motor of Electrical Vehicles Using Wavelet Transform. *IEEE Transactions on Transportation Electrification*, 3(3), pp. 694–702.
- Hang, J., Ding, S., Zhang, J., Cheng, M., Chen, W. and Wang, Q. (2016). Detection of Interturn Short-Circuit Fault for PMSM with Simple Fault Indicator. *IEEE Transactions on Energy Conversion*, 31(4), pp. 1697–1699.
- Hang, J., Sun, W., Hu, Q., Ren, X. and Ding, S. (2022). Integration of Interturn Fault Diagnosis and Fault-Tolerant Control for PMSM Drive System. *IEEE Transactions on Transportation Electrification*, 8(2), pp. 2825–2835.
- Henao, H., Capolino, G.A., Fernandez-Cabanas, M., Filippetti, F., Bruzese, C., Strangas, E., Pusca, R., Estima, J., Riera-Guasp, M., Hedayati-Kia, S. (2014). Trends in Fault Diagnosis for Electrical Machines: A Review of Diagnostic Techniques. *IEEE Industrial Electronics Magazine*, 8(2), pp. 31–42.

- Huang, W., Du, J., Hua, W. and Fan, Q. (2021). An Open-Circuit Fault Diagnosis Method for PMSM Drives Using Symmetrical and DC Components. *Chinese Journal of Electrical Engineering*, 7(3), pp. 124–135.
- Jeong, H., Moon, S., Lee, H. and Kim, S.W. (2017). Interturn short circuit fault detection of permanent magnet synchronous motors based on positive- and negative-sequence signatures. In: *Proceedings of 2017 IEEE 11th International Symposium on Diagnostics for Electrical Machines, Power Electronics and Drives (SDEMPED)*, Tinos, Greece, pp. 167–172.
- Maqsood, A., Oslebo, D., Corzine, K., Parsa, L. and Ma, Y. (2020). STFT Cluster Analysis for DC Pulsed Load Monitoring and Fault Detection on Naval Shipboard Power Systems. *IEEE Transactions on Transportation Electrification*, 6(2), pp. 821–831.
- Park, C. H., Lee, J., Ahn, G., Youn, M. and Youn, B. D. (2019). Fault Detection of PMSM Under Non-Stationary Conditions Based on Wavelet Transformation Combined with Distance Approach. In: *Proceedings of 2019 IEEE 12th International Symposium on Diagnostics for Electrical Machines, Power Electronics and Drives (SDEMPED)*, Toulouse, France, pp. 88–93.
- Pietrzak, P. and Wolkiewicz, W. (2021a). Application of Spectral and Wavelet Analysis of Stator Current to Detect Angular Misalignment in PMSM Drive Systems. *Power Electronics and Drives*, 6(41), pp. 42–60.
- Pietrzak, P. and Wolkiewicz, M. (2021b). On-line Detection and Classification of PMSM Stator Winding Faults Based on Stator Current Symmetrical Components Analysis and the KNN Algorithm. *Electronics*, 10(15), p. 1630.
- Pietrzak, P. and Wolkiewicz, M. (2021c). Comparison of Selected Methods for the Stator Winding Condition Monitoring of a PMSM Using the Stator Phase Currents. *Energies*, 14(6), p. 1630.
- Pietrzak, P. and Wolkiewicz, M. (2022). Stator winding fault detection of permanent magnet synchronous motor based on the bispectrum analysis. *Bulletin of the Polish Academy of Sciences, Technical Sciences*, 70, pp. 1–10.
- Riera-Guasp, M., Antonino-Daviu, J. A. and Capolino, G. (2015). Advances in Electrical Machine, Power Electronic, and Drive Condition Monitoring and Fault Detection: State of the Art. *IEEE Transactions on Industrial Electronics*, 62(3), pp. 1746–1759.
- Rosero, J., Cusido, J., Garcia, A., Romeral, L. and Ortega, J. A. (2007). Detection of Stator Short Circuits in PMSM by mean of joint Time-Frequency Analysis. In: *Proceedings of the 2007 IEEE International Symposium on Diagnostics for Electric Machines, Power Electronics and Drives*, Cracow, Poland, pp. 420–425.
- Rosero, J. A., Romeral, L., Ortega, J. A. and Rosero, E. (2009). Short-Circuit Detection by Means of Empirical Mode Decomposition and Wigner–Ville Distribution for PMSM Running Under Dynamic Condition. *IEEE Transactions on Industrial Electronics*, 56(11), pp. 4534–4547.
- Satpathi, K., Yeap, Y. M., Ukil, A. and Geddada, N. (2018). Short-Time Fourier Transform Based Transient Analysis of VSC Interfaced Point-to-Point DC System. *IEEE Transactions on Industrial Electronics*, 65(5), pp. 4080–4091.
- Skowron, M., Orłowska-Kowalska, T. and Kowalski, C. T. (2021). Application of Simplified Convolutional Neural Networks for Initial Stator Winding Fault Detection of the PMSM Drive Using Different Raw Signal Data. *IET Electric Power Applications*, 15, pp. 932–946.
- Skowron, M., Orłowska-Kowalska, T. and Kowalski, C. T. (2022). Detection of permanent magnet damage of PMSM drive based on direct analysis of the stator phase currents using convolutional neural network. *IEEE Transactions on Industrial Electronics*, Early Access, doi: 10.1109/TIE.2022.3146557.
- Tarchała, G., Wolkiewicz, M. and Krzysztofiak, M. (2020). Diagnosis of Short-Circuits in Induction Motor Stator Winding Using a Modified Park Transformation. *Power Electronics and Drives*, 5(41), pp. 123–133.
- Urresty, J., Riba J., Romeral, L., Roser, J. and Serna, J. (2009). Stator short circuits detection in PMSM by means of Hilbert-Huang transform and energy calculation. In: *Proceedings of International Symposium on Diagnostics for Electrical Machines, Power Electronics and Drives (SDEMPED)*, Cargese, France, pp. 1–7.
- Wolkiewicz, M., Tarchała, G., Orłowska-Kowalska, T. and Kowalski, C. T. (2016). Online Stator Interturn Short Circuits Monitoring in the DFOC Induction-Motor Drive. *IEEE Transactions on Industrial Electronics*, 63(4), pp. 2517–2528.
- Xu, B., Sun, L., Xu, L. and Xu, G. (2013). Improvement of the Hilbert Method via ESPRIT for Detecting Rotor Fault in Induction Motors at Low Slip. *IEEE Transactions on Energy Conversion*, 28(1), pp. 225–233.

-
- Zamudio-Ramírez, I., Ramirez-Nunez, J. A., Antonino-Daviu, J., Osornio-Rios, R. A., Quijano-Lopez, A., Razik, H., Romero-Troncoso, R. J. (2020). Automatic Diagnosis of Electromechanical Faults in Induction Motors Based on the Transient Analysis of the Stray Flux via MUSIC Methods. *IEEE Transactions on Industry Applications*, 56(4), pp. 3604–3613.
- Zanardelli, W. G., Strangas, E. G. and Aviyente, S. (2007). Identification of Intermittent Electrical and Mechanical Faults in Permanent-Magnet AC Drives Based on Time–Frequency Analysis. *IEEE Transactions on Industry Applications*, 43(4), pp. 971–980.
- Zhang, J., Xu, Z., Wang, J., Zhao, J., Din., Z. and Cheng, M. (2021). Detection and Discrimination of Incipient Stator Faults for Inverter-Fed Permanent Magnet Synchronous Machines. *IEEE Transactions on Industrial Electronics*, 68(8), pp. 7505–7515.
- Zhao, J., Guan, X., Li, C., Mou, Q. and Chen, Z. (2021). Comprehensive Evaluation of Inter-Turn Short Circuit Faults in PMSM Used for Electric Vehicles. *IEEE Transactions on Intelligent Transportation Systems*, 22(1), pp. 611–621.
- Zhou, X., Sun, J., Cui, P., Lu, Y., Lu, M. and Yu, Y. (2021). A Fast and Robust Open-Switch Fault Diagnosis Method for Variable-Speed PMSM System. *IEEE Transactions on Power Electronics*, 36(3), pp. 2598–2610.